



11 **Abstract**

12 Water column stratification exerts fundamental control on microbial carbon cycling in
13 oligotrophic areas of the ocean, yet its impact on the partitioning and fate of newly fixed carbon
14 remains insufficiently resolved. Here, we investigated carbon fluxes in the Northern Red Sea,
15 Gulf of Aqaba from 5 cruises conducted during the stratified period. We measured ^{14}C -based
16 measurements of primary production partitioned into particulate ($>0.7\ \mu\text{m}$; PP_{POC}) and
17 dissolved ($<0.7\ \mu\text{m}$; PP_{DOC}) fractions, bacterial production (BP), community and bacterial
18 respiration across the euphotic zone (0-100 m). As stratification intensifies and nutrient supply
19 from depth diminishes, depth-integrated PP_{POC} declined from 1.26 to 0.35 $\text{g C m}^{-2} \text{d}^{-1}$ while the
20 relative contribution of dissolved carbon pathways increases. The fraction of newly fixed
21 carbon released as dissolved organic carbon (extracellular release; PER) increased from 2.5%
22 to $>7\%$ of total PP, indicating that a larger fraction of photosynthetically fixed carbon was
23 released into the dissolved C pool. PP_{DOC} (0.02-0.03 $\text{g C m}^{-2} \text{d}^{-1}$) was positively correlated with
24 BP (0.08-0.16 $\text{g C m}^{-2} \text{d}^{-1}$), suggesting that recently released dissolved substrates contribute to
25 sustaining heterotrophic microbial activity. Despite declining primary production, BR
26 remained substantial (0.23-0.52 $\text{g C m}^{-2} \text{d}^{-1}$), resulting in low to moderate bacterial growth
27 efficiency (13-35%) and indicating that most processed carbon was respired rather than
28 incorporated into biomass. These findings indicate that summer stratification enhances the
29 relative importance of dissolved carbon release and microbial recycling, thereby reducing the
30 efficiency of carbon transfer to depth in the Gulf of Aqaba and likely other oligotrophic
31 systems.

32

33 **Key words**

34 Microbial carbon cycling; Oligotrophic seas; Primary production; Bacterial growth efficiency
35 (BGE); Extracellular carbon release (PER).



36 **1. Introduction**

37 Much of the open ocean is characterized by chronic oligotrophy, which shapes the
38 pathways and efficiency of carbon transformation in surface waters (Marañón et al., 2003;
39 Polovina et al., 2008). Under such nutrient-depleted conditions, primary production (PP) tends
40 to be low/negligible and is predominantly supported by small-celled phytoplankton that can
41 cope persistent resource limitation (Dore et al., 2008; Pennington et al., 2006; Reich et al.,
42 2022). Under such conditions, newly fixed carbon is largely retained and remineralized within
43 the microbial loop, where strong coupling between phytoplankton and bacteria controls its
44 subsequent fate (Azam and Malfatti, 2007; Zhang et al., 2025). As a result, the efficiency with
45 which carbon is transferred to higher trophic levels or exported to depth is often low (Armengol
46 et al., 2019; Alkalay et al., 2020; Roshan and DeVries, 2017; Torfstein et al., 2020).

47 The onset and relaxation of stratification largely determine how nutrients are delivered
48 to surface waters and thus govern microbial dynamics in oligotrophic environments (Dave and
49 Lozier, 2010; Reich et al., 2026; Signorini et al., 2015). With strengthening stratification, the
50 exchange between deep, nutrient-rich waters and the surface diminishes, causing nutrients in
51 the euphotic zone to become progressively depleted (Chen et al., 2021; Hazan et al., 2018;
52 Lozier et al., 2011). This imposes strong physiological constraints on phytoplankton growth
53 and activity due to limited nutrient availability (Rahav et al., 2016; Zohary et al., 2005). Under
54 these conditions, a considerable portion of newly produced organic carbon can be exuded by
55 phytoplankton as dissolved material via extracellular release (Kang et al., 2022; Morana et al.,
56 2014; Thornton, 2014). The resulting dissolved organic carbon provides a substrate for
57 heterotrophic bacteria and forms an important conduit between autotrophic production and
58 heterotrophic metabolism. This recently fixed dissolved carbon can be reused and account for
59 a substantial proportion of total carbon fixation under nutrient-limited conditions
60 (abovementioned references).

61 The fate of dissolved organic carbon in the ocean is largely determined by heterotrophic
62 bacteria, whose metabolic activity often controls whether carbon is retained within the euphotic
63 layer or transferred to depth (Baetge et al., 2021; LaBrie et al., 2022; Mentges et al., 2019).
64 Bacterial carbon uptake and respiration together define the efficiency of bacterial organic
65 carbon utilization, typically expressed as bacterial growth efficiency, BGE (del Giorgio and
66 Cole, 1998). Oligotrophic waters commonly exhibit low BGE, indicating that much of the
67 assimilated carbon is respired rather than incorporated into cellular biomass (Alothman et al.,
68 2025; Anderson and Turley, 2003; del Giorgio et al., 1997). Such conditions promote fast



69 carbon cycling within the surface ocean and further bias the system toward recycling rather
70 than export (del Giorgio and Cole, 1998). The relative magnitudes of PP and community
71 respiration (CR) therefore serve as a useful indicator of the system's metabolic status and offers
72 insight into whether the system is characterized by net carbon accumulation or rapid
73 remineralization (Izett et al., 2024; Stanley et al., 2010).

74 The Gulf of Aqaba (northern Red Sea) is an oligotrophic basin whose physical and
75 biogeochemical properties are highly affected by seasonal and interannual variability (Laiolo
76 et al., 2014; Rahav et al., 2015; Reich et al., 2024). During winter, deep convective mixing
77 injects nutrients into the surface layer, often leading to increased phytoplankton biomass and
78 productivity (Lindell and Post, 1995; Avrahami et al., 2025). Differently, in summer, a strongly
79 stratified water column results in nutrient depletion (Meder et al., 2012) and subsequently to
80 low phytoplankton biomass and activity (Lindell and Post, 1995; Reich et al., 2024). Despite
81 extensive characterization of the physical and chemical seasonal cycles in this system (Biton
82 and Gildor, 2011), the corresponding shifts in microbial carbon processing, particularly the
83 partitioning of the carbon fixed during the stratified season between particulate matter,
84 dissolved carbon released from cells, and heterotrophic utilization of this carbon, remain
85 insufficiently resolved. While the dominance of microbial recycling in oligotrophic systems
86 has long been recognized (e.g., low *f-ratios*, Alothman et al., 2025), the explicit partitioning of
87 newly fixed carbon between particulate and dissolved pathways, and its direct linkage to
88 heterotrophic metabolism across seasonal stratification, remains poorly constrained.

89 Here, we investigate microbial carbon cycling during the summer stratified period in
90 the Gulf of Aqaba, focusing on how progressive nutrient depletion influences the balance
91 between carbon fixation, release, and remineralization. To this end, we combined
92 measurements of primary production, dissolved organic carbon release, and heterotrophic
93 bacterial activity from 5 monthly cruises, to assess how the structure and efficiency of carbon
94 processing evolve over the course of the stratified season.

95

96 **2. Material and methods**

97 *2.1. Study site*

98 Seawater was collected across the euphotic zone (0-100 m) at 20 m depth intervals at an
99 offshore station in the northern Gulf of Aqaba, Red Sea (29.47°N, 34.92°E). Sampling was
100 conducted monthly from May to September 2023, spanning the transition from late spring to



101 late summer. Measurements included a comprehensive set of microbial activity measurements,
102 including particulate primary productivity ($>0.7 \mu\text{m PP}_{\text{TOT}}$), dissolved primary production
103 (PP_{DOC} , $<0.7 \mu\text{m}$), bacterial production (BP), and community respiration (CR). Ancillary data
104 comprised CTD profiles (Sea-Bird SBE 19plus), inorganic nutrients concentration, and
105 chlorophyll *a* measurements.

106

107 *2.2. Particulate and dissolved primary production and extracellular release*

108 Autotrophic activity was assessed by measuring particulate primary productivity (PP_{POC}) and
109 carbon fixed present in the dissolved fraction (PP_{DOC}), enabling a detailed partitioning of
110 carbon flow pathways within the microbial food web. To this end, seawater was collected in
111 triplicate 50 ml acid-washed Falcon tubes. The collected samples were spiked with $\text{NaH}^{14}\text{CO}_3$
112 (Perkin Elmer, specific activity 56 mCi mmol^{-1}) at a final radioisotope dilution of $1:10^4 \text{ v.v}$ (1
113 $\mu\text{Ci}/10 \text{ ml}$) and incubated for 24 h under ambient temperature and light. Incubations were
114 stopped by filtration of the ^{14}C -enriched water samples through GF/F filters ($0.7 \mu\text{m}$ nominal
115 pore size, PP_{POC}) using low vacuum pressure ($<50 \text{ mmHg}$). Filtrate material samples (5-10 ml,
116 PP_{DOC}) were also collected in 15 ml Faclon tubes. Filters were rinsed with 5 ml of sterile-
117 filtered seawater collected from the same site ($<0.2 \mu\text{m}$) and the samples were subsequently
118 acidified with 50 μl of 37% hydrochloric acid to remove inorganic carbon overnight. Filters
119 were transferred into glass vials and 5 ml of scintillation cocktail (Ultima Gold) was added. To
120 determine PP_{DOC} , the filtrate (10 ml) was transferred to scintillation vials, acidified with 50 μl
121 hydrochloric acid and 5ml scintillation cocktail was added as above. Samples were counted
122 using a TRI-CARB 4810 TR (Packard) liquid scintillation counter. Blank samples (for both
123 PP_{POC} and PP_{DOC}) collected from each depth were spiked with $\text{NaH}^{14}\text{CO}_3$ and filtered
124 immediately without incubation. These blanks yielded negligible counts, and their reads were
125 subtracted from their respective samples read. Added activity of the radiolabeled ‘working
126 solution’ was obtained in each campaign by removing 50 μl from random samples immediately
127 after spiking and before incubation (usually one per sampling depth), placing it on a new GF/F
128 filter, adding 50 μl ethanolamine (a strong base that prevent bicarbonate evaporation) and
129 scintillation liquid, and counting immediately. The variability between the ‘added activity’
130 measurements was usually negligible for the same work solution (prepared freshly before each
131 campaign), and we therefore used the average value of all collected samples/depths on each
132 cruise.



133 PP_{POC} and PP_{DOC} rates were calculated based on the Bermuda Atlantic Time-series
134 Study (BATS) protocol (<https://www.bco-dmo.org/dataset/893182/description#acquisition>)
135 using the equation:

$$136 \quad (1) \text{ Primary productivity} = \frac{(\text{DPM} - \text{blank})}{V} \times \text{DIC} \times \frac{\text{AA vol}}{\text{TDPM}} \times f \times \frac{1}{t}$$

137 Where, DPM equals the disintegrations per minute, V = the filtered volume, DIC is the
138 dissolved inorganic carbon in seawater calculated from total alkalinity; $\sim 25 \mu\text{g C L}^{-1}$, AA vol
139 = Added activity volume, TDPM = Total ^{14}C disintegration per minute, t = incubation time, and
140 f = factor correcting the uneven uptake of ^{14}C due to fractionation (1.05).

141 The percentage of extracellular release (PER; %) was calculated as follows:

$$142 \quad (2) \text{ PER (\%)} = \frac{\text{PP}_{\text{DOC}}}{\text{PP}_{\text{POC}} + \text{PP}_{\text{DOC}}} \times 100$$

143

144 2.3. Bacterial productivity (BP)

145 Triplicate seawater samples (1.7 ml) from each sampling depth were incubated in the dark
146 under ambient temperature with 10 nmol L⁻¹ of ^3H -leucine (Perkin Elmer; specific activity 123
147 Ci mmol⁻¹) for 4 h at *in situ* temperature, following the protocol of Simon et al., (1990).
148 Incubations were terminated by the addition of 100 μl of 100% trichloroacetic acid, and
149 samples were subsequently processed using the microcentrifugation method (Smith and Azam,
150 1992). After processing, 1 ml of scintillation cocktail (Ultima Gold) was added to each vial,
151 and radioactivity was measured using a TRI-CARB 4810 TR (Packard) liquid scintillation
152 counter. Random 'killed' controls, containing ^3H -leucine and trichloroacetic acid added prior
153 to incubation were used to account for background activity. Leucine incorporation rates were
154 converted to carbon production using a conversion factor of 3 kg C mol⁻¹ leucine, assuming an
155 isotopic dilution factor of 2 (Simon and Azam, 1989).

156

157 2.4. Community and bacterial respiration

158 Community respiration (CR) rates were estimated from dark triplicate incubations per depth
159 under ambient temperature. Dissolved O₂ concentrations were measured using an optical
160 oxygen meter (FireSting, PyroScience GmbH) equipped with fiber-optic sensors. Prior to the
161 incubations, optical sensor spots (OXSP5, PyroScience) were affixed to the inner wall of
162 Winkler bottles (300 ml) according to the manufacturer's instructions. Bottles were carefully
163 filled to avoid bubble formation and sealed with ground-glass stoppers. Samples were
164 incubated for 24 h under continuous, gentle stirring using magnetic stir bars to ensure



165 homogeneous O₂ distribution without introducing air bubbles or disturbing the sensor spot. The
166 system was calibrated prior to measurements using a two-point calibration (air-saturated
167 seawater and zero-oxygen solution) following the manufacturer's guidelines. CR was
168 calculated as the temporal change in O₂ concentration (T₂₄ minus T₀) normalized to the
169 incubation duration (Cheung et al., 2024). The detection limit was 0.5 μmol O₂ L⁻¹. CR was
170 converted into bacterial respiration (BR) using the linear regression of Aranguren-Gassis et al.,
171 (2012):

$$(3) BR = 0.3 \times CR^{1.22} - 0.013$$

172
173
174 A respiratory quotient of 1 was used to convert O₂ consumption into carbon respiration (del
175 Giorgio and Cole, 1998). Bacterial gross efficiency (BGE) was calculated as follows (del
176 Giorgio and Cole, 1998):

$$(4) BGE (\%) = \frac{BP}{BP + BR} \times 100$$

177
178

179 2.5. Inorganic nutrients

180 Samples were collected in acid-washed plastic Falcon tubes and kept frozen at -20 °C until
181 analysis within a few months. One sample per depth was collected. Nitrate+nitrite (NO₂+NO₃),
182 orthophosphate (PO₄) and Si(OH)₄ were measured with a Seal Analytical AA-3 system (Kress
183 and Herut, 2001). The limits of detection (twice the standard deviation of the blank) were 0.03
184 μM for nitrate+ nitrite, 0.008 μM for orthophosphate, and 0.05 μM for silicic acid. Ammonium
185 (NH₄) concentrations were measured fluorometrically using the orthophthaldialdehyde (OPA)
186 method (Holms et al., 1999) using a Turner Designs (Trilogy) fluorometer equipped with 365-
187 nm excitation and 460-nm emission filters. The detection limit was 0.01 μM. The quality of
188 the nutrient measurements is regularly confirmed by inter-comparison exercises (e.g.,
189 QUASIMEME program).

190

191 2.6. Chlorophyll a

192 Seawater (300 ml) were filtered through GF/F and stored at -20 °C in a dark box. One sample
193 per depth was collected. Samples were extracted overnight in 5 ml of 90% acetone at 4 °C in
194 the dark (Welschmeyer, 1994). Chlorophyll concentrations were determined using a Turner
195 Designs (Trilogy) fluorometer with 436-nm excitation and 680-nm emission filters.

196

197 2.7. Statistical analyses



198 Pairwise relationships among environmental and biological variables were assessed using
199 Pearson correlation analysis. All data points from the upper 0–100 m across the five sampling
200 campaigns were included. Prior to analysis, data were screened for missing values, and only
201 complete datasets were retained. Pearson correlation coefficients (r) and corresponding p -
202 values were calculated to assess the strength and significance of pairwise relationships.
203 Statistical significance was evaluated at two levels ($p < 0.05$ and $p < 0.01$). Correlation matrices
204 were visualized using a lower-triangle format to improve readability, with color gradients
205 representing correlation strength and overlaid values indicating correlation coefficients and
206 their significance levels. Analyses and figure generation were performed using Python (version
207 3.13).

208

209 3. Results

210 Surface waters (0–20 m) were consistently warm throughout the study period (25–28
211 °C) and showed a clear seasonal increase in temperature from early to mid-summer (Figure
212 1A). The mixed layer depth (MLD), estimated from a temperature threshold criterion ($\Delta T =$
213 0.2 °C from surface values, de Boyer Montégut et al., 2004), shoaled progressively from 45 m
214 in early summer (May) to 15–20 m during peak stratification (July–August), before slightly
215 deepening again in September (28 m). A pronounced vertical temperature gradient was evident
216 throughout the sampling period, with temperatures decreasing to 23–24 °C at 100 m (Figure
217 1A). Inorganic nutrient concentrations were generally low throughout the upper water column
218 and increased with depth across the 0–100 m layer (Figure 1B–D). Nitrate+nitrite ($\text{NO}_3 + \text{NO}_2$)
219 concentration ranged from below detection level ($< 0.03 \mu\text{mol L}^{-1}$) to $0.14 \mu\text{mol L}^{-1}$ (Figure
220 1B), resulting in integrated values of $4.5\text{--}11.2 \mu\text{mol m}^{-2}$ (Table 1). $\text{NO}_3 + \text{NO}_2$ concentrations
221 were only slightly higher below the MLD (Figure 1B), indicating restricted nutrient supply
222 from the nutricline to the upper euphotic zone during summertime. Ammonium (NH_4)
223 concentrations were also low, ranging from 12 to 65 nmol L^{-1} , and increased with depth (Figure
224 1C). Depth-integrated NH_4 concentrations were higher during mid- to late summer ($3.0\text{--}4.6$
225 $\mu\text{mol m}^{-2}$) compared to early summer ($1.7 \mu\text{mol m}^{-2}$; Table 1). Orthophosphate (PO_4) was
226 usually low throughout the water column and across all sampling periods; $0.01\text{--}0.03 \mu\text{mol L}^{-1}$,
227 with the exception of a single elevated surface value of $0.07 \mu\text{mol L}^{-1}$ observed during the
228 September cruise (Figure 1D). The integrated PO_4 was low and ranged from $2.1\text{--}4.3 \mu\text{mol m}^{-2}$
229 (Table 1). The resulting N:P ratio was below the canonical Redfield ratio of 16:1 (Redfield,
230 1934) and ranged from 1.8:1 to 7.5:1 (Table 1), suggesting N limiting conditions for the
231 microbial populations (Tanioka et al., 2022). Silicic acid ($\text{Si}(\text{OH})_4$) concentrations were



232 relatively homogeneous throughout the water column (Figure 1E). However, higher levels were
233 observed in May-June ($1 \mu\text{mol L}^{-1}$, $75\text{-}89 \mu\text{mol m}^{-2}$), followed by a decline during July-
234 September ($<0.6 \mu\text{mol L}^{-1}$, $55 \mu\text{mol m}^{-2}$) (Figure 1E, Table 1), suggesting a transition from a
235 diatom-influenced system in spring/early summer to an oligotrophic, small-cell-dominated
236 community under more stratified conditions (Avrahami et al., 2025).

237 Chlorophyll *a* exhibited a pronounced vertical structure across all sampling periods
238 (Figure 2A). Where surface concentrations were typically low, ranging from 0.05 to $0.15 \mu\text{g L}^{-1}$,
239 and increased with depth to form a well-defined deep chlorophyll maximum (DCM). The
240 DCM was consistently located between 60 and 100 m, coinciding with the lower euphotic zone.
241 Chlorophyll concentrations at the DCM ranged from 0.3 to $0.7 \mu\text{g L}^{-1}$, representing a several-
242 fold increase relative to surface waters. Vertically integrated chlorophyll biomass (0-100 m)
243 ranged from 16 to 28mg m^{-2} across the study period (Table 1). Integrated biomass was lowest
244 in early summer (May-June; $16\text{-}20 \text{mg m}^{-2}$) and increased toward mid/late-summer (July-
245 September; $25\text{-}28 \text{mg m}^{-2}$).

246 Particulate primary production (PP_{POC}) exhibited a pronounced vertical gradient across
247 all sampling periods, with highest rates observed in surface waters and a progressive decline
248 with depth (Figure 2B). Surface PP_{POC} ranged from $25 \mu\text{g C L}^{-1} \text{d}^{-1}$ in early summer and
249 decreased to $8 \mu\text{g C L}^{-1} \text{d}^{-1}$ during mid- to late summer (Figure 2B). Below 40-60 m, PP_{POC}
250 declined substantially in all stations and ranged from $8 \mu\text{g C L}^{-1} \text{d}^{-1}$ in May to $1 \mu\text{g C L}^{-1} \text{d}^{-1}$ in
251 June-September to (Figure 2B). Depth-integrated PP_{POC} ranged from 0.28 to $1.26 \text{g C m}^{-2} \text{d}^{-1}$
252 (Table 1), with the highest PP_{POC} values observed in early summer (May), followed by a
253 marked decline toward mid-summer (June-August), and a slight increase in September. This
254 seasonal decrease in integrated PP_{POC} coincided with the progressive shoaling of the mixed
255 layer (Table 1, Figure 1A) and reduced nutrient availability in surface waters (Figure 1B-E),
256 and is in agreement with previous observations in the area (Iluz et al., 2009; Reich et al., 2024).
257 PP_{DOC} generally displayed its highest rates in the upper water column (Figure 2C). In June-
258 September, PP_{DOC} was elevated in surface and near-surface waters, typically ranging from 0.2
259 to $0.5 \mu\text{g C L}^{-1} \text{d}^{-1}$, and then declined progressively with depth. Below 80 m, rates were
260 consistently lower than $0.10 \mu\text{g C L}^{-1} \text{d}^{-1}$. In contrast, the May profile was uniform throughout
261 the water column ($0.4 \mu\text{g C L}^{-1} \text{d}^{-1}$). Despite these differences in vertical distribution, depth-
262 integrated PP_{DOC} varied only slightly across months, ranging from 0.02 to $0.03 \text{g C m}^{-2} \text{d}^{-1}$
263 (Table 1). The percentage of extracellular organic carbon release (PER) increased over the
264 course of the summer and showed a clear depth dependence (Figure 2D). In May, PER was



265 generally low and relatively uniform (<5%), consistent with the homogeneous distribution of
266 P_{DOC} (Figure 2C). In contrast, from June onward PER was lower in the upper water column
267 (<10%) and increased with depth, with the highest values typically observed below 40-60 m,
268 near the base of the euphotic zone reaching as high as 20%. Integrated PER rose from 2.5% in
269 May to 5.7-6.4% during June-August and reached 7.4% in September (Table 1).

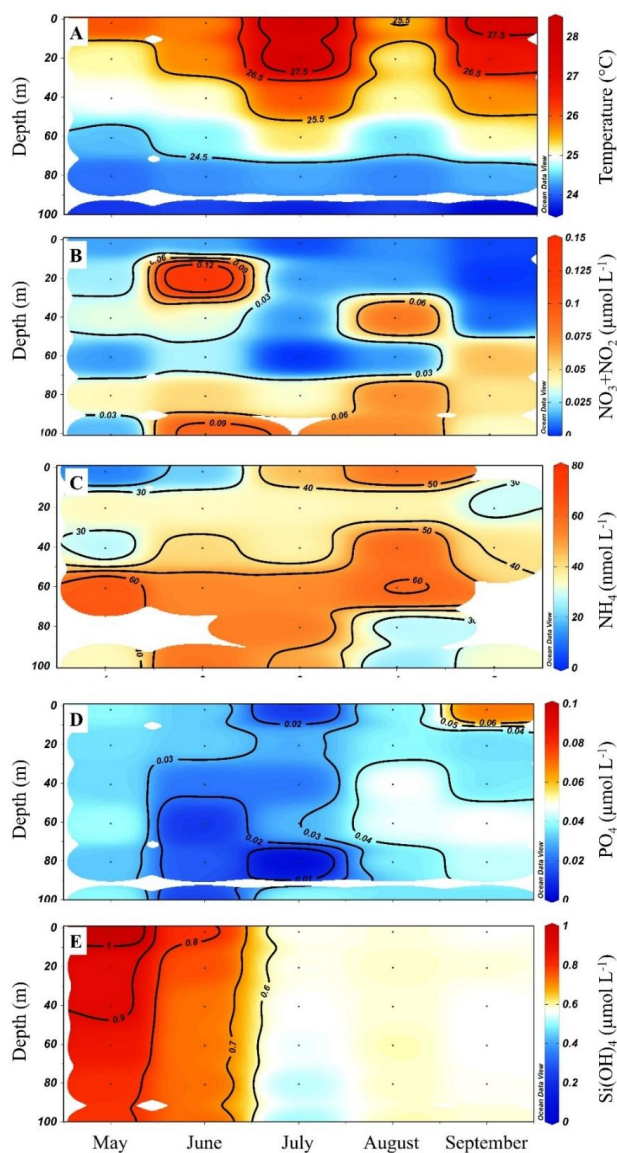
270 Heterotrophic prokaryotic (bacterial) production (BP) exhibited moderate vertical and
271 temporal variability (Figure 3A). Where BP rates were generally highest in the upper water
272 column (0-40 m), ranging from 0.8 to 2.5 $\mu\text{g C L}^{-1} \text{d}^{-1}$, and declined with depth. Below 60-80
273 m, BP decreased substantially, with values commonly $<1 \mu\text{g C L}^{-1} \text{d}^{-1}$ near the base of the
274 euphotic zone. Depth-integrated BP ranged from 0.08 to 0.16 $\text{g C m}^{-2} \text{d}^{-1}$ across the study
275 period, with the higher values observed during mid- to late summer (Table 1). Bacterial
276 respiration (BR) was high and relatively homogeneous throughout the water column in May-
277 June, with rates typically around 4-8 $\mu\text{g C L}^{-1} \text{d}^{-1}$ (Figure 3B), summing to 0.4-0.5 $\text{g C m}^{-2} \text{d}^{-1}$
278 over the upper 100 m (Table 1). Differently, during July-August, BR exhibited a stronger
279 vertical variability with higher respiration rates recorded in the upper 40-60 m (4-5 $\mu\text{g C L}^{-1} \text{d}^{-1}$
280 ¹) and lower at the bottom of the euphotic layer around 0-40 m (1-2 $\mu\text{g C L}^{-1} \text{d}^{-1}$). In September,
281 BR again showed relatively low vertical variability, with rates mostly between 1 and 4 $\mu\text{g C L}^{-1}$
282 ¹ d^{-1} , corresponding to 0.25 $\text{g C m}^{-2} \text{d}^{-1}$.

283 The spatial and vertical distribution of bacterial growth efficiency (BGE, Figure 3C)
284 broadly mirrored that of BR (Figure 3B) and was consistent with patterns observed for BP
285 (Figure 3A). In all months, relatively higher BGE values were found in the upper 0-60 m,
286 whereas lower values were typically observed at greater depths (Figure 3C). Temporally, BGE
287 was lower during May-June, when values throughout the water column were typically 10-20%
288 (integrated value 13%, Table 1), reflecting the relatively high and vertically homogeneous BR
289 during this period (Figure 3C). In contrast, from July onward, BGE increased in the upper water
290 column, commonly reaching 20-40% in the 0-60 m layer and 10-20% below 60 m (Figure 3C),
291 summing 28-30% over the whole euphotic layer (Table 1). In September, BGE exhibited
292 reduced vertical variability, with values generally ranging between 15 and 30% across the water
293 column (Figure 3C).

294 Pearson correlation analysis revealed that depth and temperature were the dominant
295 structuring variables, with depth negatively correlated with temperature ($r=-0.83$, $p<0.01$) and
296 strongly positively correlated with chlorophyll *a* ($r=0.89$, $p<0.01$), reflecting the vertical

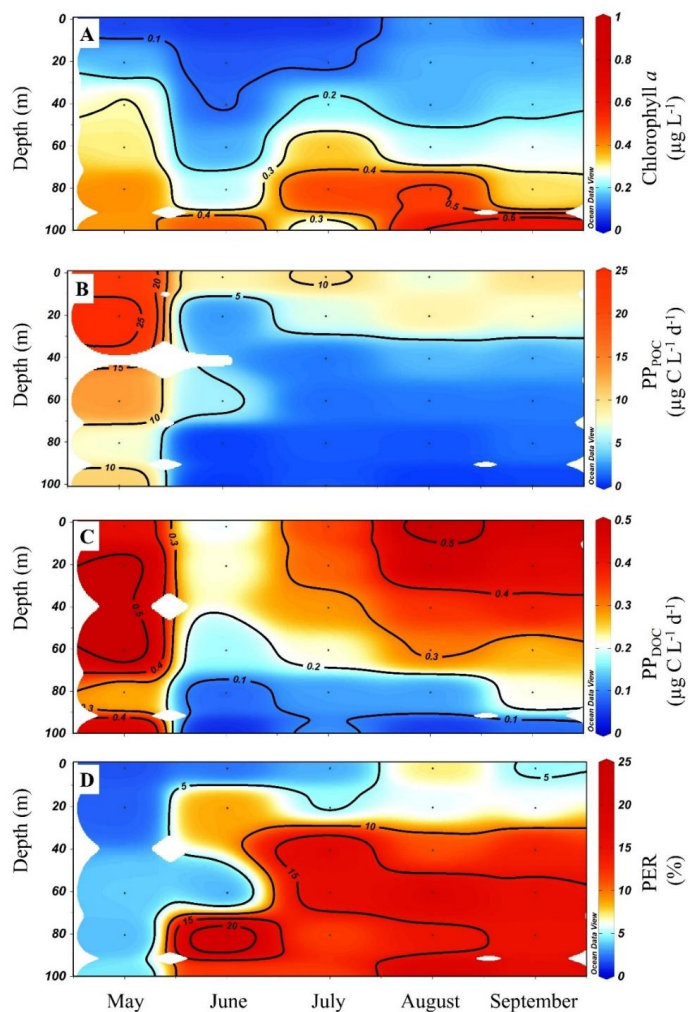


297 separation between surface waters and the DCM (Figure 4). Depth was also negatively
298 correlated with both PP_{POC} ($r=-0.54$, $p<0.01$) and PP_{DOC} ($r=-0.63$, $p<0.01$) (Figure 4),
299 indicating that autotrophic activity was mainly concentrated in the upper euphotic zone (Figure
300 2B,C). As expected, PP_{POC} positively correlated with PP_{DOC} ($r=0.69$, $p<0.01$) (Figure 4),
301 demonstrating that the release of dissolved organic carbon scales with total photosynthetic
302 activity. At the same time, PP_{POC} showed a significant negative correlation with chlorophyll *a*
303 ($r=-0.46$, $p<0.05$) (Figure 4), suggesting a decoupling between biomass accumulation and
304 photosynthetic rates as found for chlorophyll *a* (Figure 2). Interestingly, PP_{DOC} exhibited
305 several key relationships that highlight its central role in carbon cycling in the Gulf of Aqaba
306 during summertime. For example, PP_{DOC} was positively correlated with PO_4 ($r=0.47$, $p<0.05$),
307 and negatively correlated with chlorophyll *a* ($r=-0.58$, $p<0.01$) (Figure 4). These patterns
308 indicate that PO_4 may be preferentially regenerated from following the DOC released from the
309 cells. Furthermore, PP_{DOC} was positively correlated with BP ($r=0.50$, $p<0.01$) (Figure 4),
310 supporting the role of PP_{DOC} as an important substrate fueling heterotrophic activity in the Gulf
311 of Aqaba. In contrast, inorganic nitrogen species (e.g., NO_3+NO_2 , NH_4) showed weak or non-
312 significant relationships with PP_{POC} or PP_{DOC} (Figure 4), suggesting these N species are utilized
313 as fast as they released from cells or that they are not released as much as carbon and
314 orthophosphate.



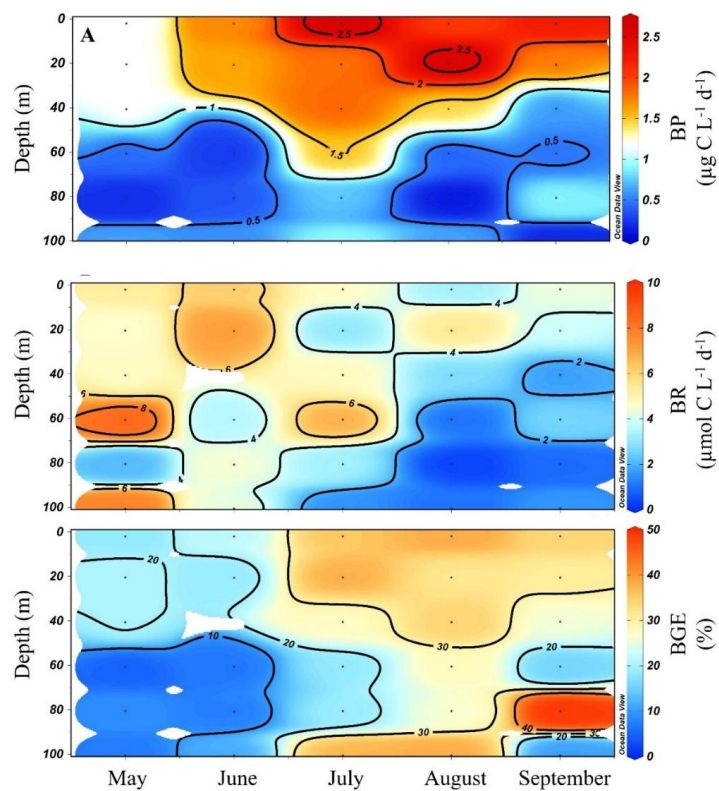
315

316 **Figure 1:** Depth distribution of temperature (A), NO₂+NO₃ (B), NH₄ (C), PO₄ (D) and Si(OH)₄
317 (E) in the upper water column (0-100 m) of the Gulf of Aqaba during summertime (May to
318 September).



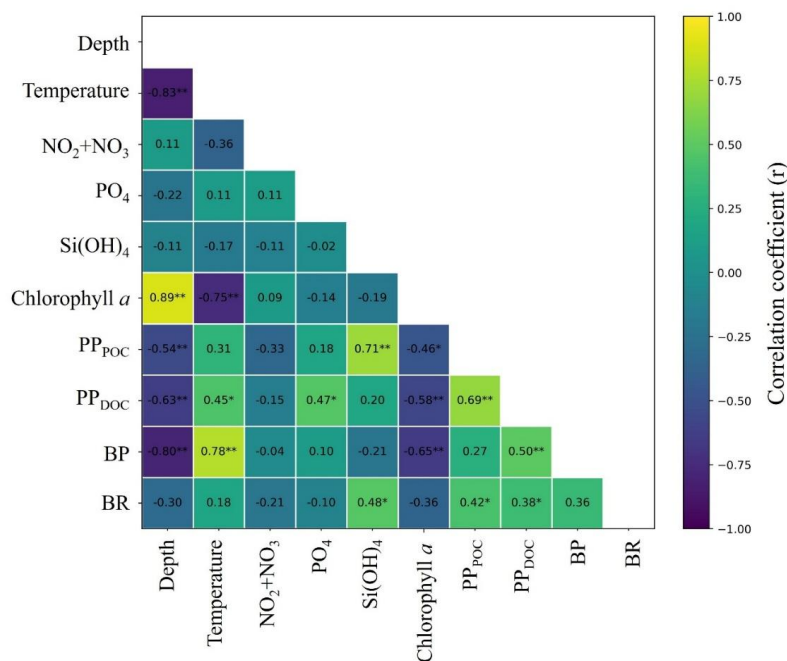
319

320 **Figure 2:** Depth distribution of chlorophyll a (A), PP_{POC} (B) PP_{DOC} (C) and the percentage of
321 extracellular release, PER (D) in the upper water column (0-100 m) of the Gulf of Aqaba during
322 summertime (May to September).



323

324 **Figure 3:** Depth distribution of bacterial productivity, BP (A), bacterial respiration, BR (B),
325 and bacterial gross efficiency, BGE (C) in the upper water column (0-100 m) of the Gulf of
326 Aqaba during summertime (May to September).



327

328 **Figure 4:** Pearson correlation matrix of physical, chemical, and biological variables measured
 329 in the upper 0–100 m of the water column. Colores indicate the strength and direction of the
 330 correlation (Pearson’s *r*), and values within each cell represent correlation coefficients.
 331 Statistical significance is indicated as **p*<0.05 and ***p*<0.01. The analysis is based on all
 332 depth-resolved measurements across the five cruises (May to September).



333 **Table 1:** Summary of integrated values (0-100 m) measured in the Gulf of Aqaba during the
334 summer.

	May	June	July	August	September
Mixed layer depth (m)	45	31	21	15	28
NO ₃ +NO ₂ ($\mu\text{mol m}^{-2}$)	4.5	11.2	7.5	7.8	6.0
NH ₄ ($\mu\text{mol m}^{-2}$)	1.7	4.5	4.6	3.4	3.0
PO ₄ ($\mu\text{mol m}^{-2}$)	3.5	2.1	2.1	4.1	4.3
DIN/PO ₄ (ratio)*	1.8	7.5	5.8	2.7	2.1
Si(OH) ₄ ($\mu\text{mol m}^{-2}$)	89	75	55	59	57
PP _{POC} (g C m ⁻² d ⁻¹)	1.26	0.28	0.34	0.37	0.39
PP _{DOC} (g C m ⁻² d ⁻¹)	0.03	0.02	0.02	0.03	0.03
PER (%)	2.5	5.7	5.6	6.4	7.4
BP (g C m ⁻² d ⁻¹)	0.08	0.08	0.16	0.12	0.10
CR (g C m ⁻² d ⁻¹)	1.03	1.01	0.86	0.50	0.53
BR (g C m ⁻² d ⁻¹)	0.52	0.51	0.42	0.23	0.24
BGE (%)	13.5	13.1	27.7	34.1	29.8
PP _{TOT} /CR (ratio)**	1.26	0.30	0.42	0.78	0.78

335 * DIN = NH₄+NO₃+NO₂

336 ** PP_{TOT} = PP_{POC}+PP_{DOC}



337 **4. Discussion**

338 *4.1. Summer stratification shifts carbon cycling toward dissolved pathways*

339 The Gulf of Aqaba exhibits strong seasonal hydrographic variability with deep winter
340 mixing followed by stable stratification afterward (Biton and Gildor, 2011), leading to nutrient-
341 depleted surface water throughout the summer months (Laiolo et al., 2014; Meeder et al.,
342 2012). The shift from deeply mixed winter conditions to a strongly stratified summer water
343 column substantially reshapes autotrophic production, heterotrophic activity, and the efficiency
344 with which carbon is exported from the surface (Karl et al., 2021). Understanding how
345 microbial communities adjust their carbon-use strategies under nutrient-poor conditions is
346 therefore important for predicting the fate of newly fixed carbon in stratified and oligotrophic
347 oceans.

348 The progressive shoaling of the mixed layer from early to late summer (Table 1),
349 together with persistently low nutrient concentrations and reduced nutrient inventories (Figure
350 1B-E), indicates increasing isolation of the euphotic zone from the nutricline, typically located
351 at depths >150 m in this region (Landou et al., 2023; Meeder et al., 2012; Rahav et al., 2015).
352 As stratification intensified, depth-integrated primary production declined from early to mid-
353 summer, while chlorophyll biomass became increasingly concentrated within a pronounced
354 DCM (Figure 2A). This decoupling between biomass and productivity is consistent with a
355 community persisting under chronic low nutrient availability, maintaining low standing stocks
356 but operating at reduced photosynthetic efficiency (Marañón et al., 2010). At the same time,
357 the vertical distributions of PP_{DOC} and PER indicate a shift in carbon allocation within the water
358 column (Figure 2). Where PP_{DOC} remains concentrated in the upper water column and is
359 relatively stable over the season, while PER increases both with depth and over time, reaching
360 its highest values under the strongest stratification (Figure 2). This pattern implies that an
361 increasing fraction of newly fixed carbon was released as DOC in the upper 100 m, especially
362 as summer progressed and as imbalances between carbon fixation and nutrient assimilation
363 limited biomass synthesis and ‘favored’ the exudation of photosynthates (Mueller et al., 2016;
364 Ofaim et al., 2021). Under such conditions, excess carbon leaks or excreted as low-molecular-
365 weight compounds, thus elevating PER and enhancing the supply of labile dissolved organic
366 substrates to heterotrophic prokaryotes (Engel et al., 2017, 2014, 2004). Consequently, a larger
367 share of PP_{TOT} was routed into the microbial loop rather than retained in particulate autotrophic
368 biomass (i.e., PP_{POC}), enhancing carbon recycling and reducing the efficiency of export to depth
369 (Table 1; Carlson et al., 2010).



370 The increasing release of newly fixed carbon as dissolved organic matter thus provides
371 a key link between autotrophic production and sustained heterotrophic activity within the
372 euphotic zone, even as primary production declines over the summer (Table 1, Figure 2). In
373 oligotrophic systems such as the Gulf of Aqaba, heterotrophic microbial communities are often
374 tightly coupled to DOC supply derived from contemporaneous primary production as well as
375 semi-labile DOC that accumulates over seasonal timescales (Hansell et al., 2009; Santinelli,
376 2015). The persistence of BP in our study suggests that microbial metabolism is supported by
377 a combination of freshly released DOC, recycled organic matter, and/or external nutrient inputs
378 such as those added from aerosol deposition (Paytan et al., 2009; Rahav et al., 2018). Similar
379 accumulated DOC and associated impacts on the microbial community have been observed in
380 other stratified regions, where semi-labile DOC mitigates temporal imbalances between
381 production and consumption (Hansell et al., 2009; Hansell and Carlson, 2002). In contrast, a
382 recent study in the Eastern Tropical North Atlantic reported that BP and BR closely follow
383 PP_{TOT} concentrations, which are dominated by semi-labile DOC, with PP_{DOC} supply often
384 exceeded bacterial carbon demand (Devresse et al., 2022). There, heterotrophic activity was
385 largely controlled by and coupled to contemporaneous production, resulting in a production-
386 driven carbon cycle. In the Gulf of Aqaba, however, the weaker coupling between PP_{TOT} and
387 heterotrophic activity points to a recycling-dominated regime in which microbial communities
388 increasingly depend on internally regenerated carbon and are not directly linked to
389 contemporaneous production. Under sustained stratification, reduced nutrient supply
390 constrains autotrophic growth while promoting DOC release and accumulation, thereby
391 maintaining BR even as primary production declines (Hansell et al., 2009; Hansell, 2013). The
392 low BGE observed (Table 1, Figure 3C) further support this view, indicating that most of the
393 consumed carbon is respired rather than converted into biomass, a characteristic of strongly
394 recycling systems in oligotrophic ocean settings (del Giorgio and Cole, 1998). Indeed, the
395 vertical structure of BGE closely mirrors that of BR, indicating that most of the organic carbon
396 processed by heterotrophic prokaryotes was respired rather than incorporated into new
397 biomass. These low growth efficiencies are consistent with the energetic constraints typical of
398 oligotrophic waters, indicating that bacterial carbon use was directed mainly toward respiration
399 rather than growth, with much of the organic carbon rapidly returned to dissolved inorganic
400 form (del Giorgio and Cole, 1998).

401

402 *4.2. Potential drivers of microbial carbon processing in the Gulf of Aqaba during summertime*



403 The observed vertical patterns in microbial carbon cycling are primarily structured by
404 gradients in light availability/nutrient supply and stratification intensity, which all co-vary with
405 depth (Figure 4). Where, chlorophyll *a* peaks at the DCM, reflecting enhanced biomass
406 accumulation at depth, while rates of PP_{TOT} , PP_{DOC} , and BP are highest in the upper, well-lit
407 layers. This pattern suggests that while biomass is concentrated near the DCM, much of the
408 carbon fixation, release, and recycling occur in the upper euphotic zone. Within this framework,
409 a strong coupling between PP_{POC} and PP_{DOC} would suggest that dissolved carbon release scales
410 directly with photosynthetic activity, consistent with extracellular release as an inherent
411 component of primary production under oligotrophic conditions. However, the negative
412 relationship between both PP_{POC} and PP_{DOC} with chlorophyll *a* (Figure 4) indicates that carbon
413 fixation and release are not directly linked to standing stock of biomass, but rather to
414 physiological activity in the upper water column (Figure 2). Importantly, PP_{DOC} showed a
415 stronger association with BP than PP_{POC} does, emphasizing the central role of dissolved organic
416 carbon in sustaining heterotrophic metabolism. This supports the idea that the microbial loop
417 in the Gulf of Aqaba is primarily fueled by recently produced dissolved substrates rather than
418 by particulate pathways (abovementioned references). In contrast, the weak/no correlations
419 between nutrients and biological rates, attributed by their rapid uptake, suggest that nutrient
420 distributions are largely governed by vertical mixing rather than biological uptake.

421 Together, these patterns indicate that carbon cycling in the Gulf of Aqaba is structured
422 by two complementary processes: (i) vertical decoupling between biomass accumulation and
423 carbon cycling activity driven by stratification, and (ii) tight coupling between dissolved carbon
424 production and heterotrophic utilization (Figure 4). That is in the surface layer fixed carbon
425 fuels biomass activity of both fixation and respiration with no increase in biomass due to rapid
426 recycled of the carbon while deeper in the euphotic zone at the DCM fixed carbon contributes
427 to increase in biomass and particulate carbon sinking to depth. This duality reinforces the view
428 of a recycling-dominated system in which dissolved pathways, rather than particulate export,
429 regulate the fate of fixed carbon in the upper photic zone.

430

431 **5. Conclusions**

432 Our observations provide a quantitative and process-based framework for
433 understanding how stratification restructures carbon flow, showing that the Gulf of Aqaba
434 system shifts from particulate production toward sustained dissolved carbon release that
435 maintains heterotrophic metabolism despite declining primary production. As climate-driven
436 warming intensifies the density barriers of low- and mid-latitude pelagic systems (Duarte et



437 al., 2013), nutrient recycling rates are expected to become more prevalent, potentially
438 enhancing DOC turnover, thus lowering carbon export efficiency, and strengthening the role of
439 the microbial loop in regulating air-sea CO₂ exchange. Thus, increased stratification may lead
440 to longer residence times of organic carbon in the surface ocean (through multiple regeneration
441 and utilization cycles), tighter microbial coupling to DOC, and an expansion of BR relative to
442 BP, with implications for nutrient regeneration, and ecosystem structure, including shifts
443 toward smaller phytoplankton and more efficient recyclers.

444 Future work should explicitly link physical forcing, nutrient inputs, and microbial
445 carbon partitioning across seasonal to interannual scales in the Gulf of Aqaba and other
446 oligotrophic basins. Long-term observations and targeted experiments that manipulate
447 stratification, nutrient supply, and temperature will be essential to predict how microbial
448 communities adjust DOC release, BGE, and BR under progressing oligotrophication.
449 Integrating field measurements with trait-based and ecosystem models could help quantify how
450 shifts in microbial carbon dynamics under enhanced stratification alter the efficiency of the
451 biological carbon pump and feedback to climate, including potential interactions with aerosol
452 inputs and emerging stressors such as acidification and deoxygenation.

453

454 **Data Availability Statement**

455 All the data is presented in the graphs/table/text and will be made available in excel format
456 upon request.

457

458 **Credit Authorship Contribution Statement**

459 Conceptualized and conducted the field measurements; ER. Data curation, formal analysis, and
460 visualization; ER, and AP. The paper was prepared by ER and AP.

461

462 **Acknowledgments**

463 The authors thank the personnel from the Israeli National Monitoring project of Eilat and the
464 Inter University Institute for Marine Sciences in Eilat (IUI).

465

466 **Funding**

467 This paper was partly supported by a grant from the Middle East Regional Cooperation
468 (MERC) (M39-011) to ER and AP.

469

470



471 **References**

- 472 Alkalay, R., Zlatkin, O., Katz, T., Herut, B., Halicz, L., Berman-Frank, I., Weinstein, Y.,
473 2020. Carbon export and drivers in the southeastern Levantine Basin. *Deep. Res. Part II*
474 *Top. Stud. Oceanogr.* 171, 104713. <https://doi.org/10.1016/j.dsr2.2019.104713>
- 475 Alothman, A., Duarte, C.M., Qurban, M.A., Agustí, S., 2025. Flow of heterotrophic
476 production in oligotrophic ocean waters. *Front. Microbiol.* 16, 1530627.
477 <https://doi.org/10.3389/fmicb.2025.1530627>
- 478 Anderson, T.R., Turley, C.M., 2003. Low bacterial growth efficiency in the oligotrophic
479 eastern Mediterranean Sea: a modelling analysis. *J. Plankton Res.* 25, 1011–1019.
480 <https://doi.org/10.1093/plankt/25.9.1011>
- 481 Aranguren-Gassis, M., Teira, E., Serret, P., Martínez-García, S., Fernández, E., 2012.
482 Potential overestimation of bacterial respiration rates in oligotrophic plankton
483 communities. *Mar. Ecol. Prog. Ser.* 453, 1–10.
- 484 Armengol, L., Calbet, A., Franchy, G., Rodríguez-Santos, A., Hernández-León, S., 2019.
485 Planktonic food web structure and trophic transfer efficiency along a productivity
486 gradient in the tropical and subtropical Atlantic Ocean. *Sci. Rep.* 9, 2044.
487 <https://doi.org/10.1038/s41598-019-38507-9>
- 488 Avrahami, Y., Koplovitz, G., Frada, M.J., 2025. Diatom community succession and bloom
489 variability as a function of winter-mixing depth in the subtropical Gulf of Aqaba, Red
490 Sea. *Mar. Ecol. Prog. Ser.* 760, 39–54.
- 491 Azam, F., Malfatti, F., 2007. Microbial structuring of marine ecosystems. *Nat. Rev.*
492 *Microbiol.* 5, 782–91. <https://doi.org/10.1038/nrmicro1747>
- 493 Baetge, N., Behrenfeld, M.J., Fox, J., Halsey, K.H., Mojica, K.D.A., Novoa, A., Stephens,
494 B.M., Carlson, C.A., 2021. The seasonal flux and fate of dissolved organic carbon
495 through bacterioplankton in the Western North Atlantic. *Front. Microbiol.* 12, 669883.
496 <https://doi.org/10.3389/fmicb.2021.669883>
- 497 Biton, E., Gildor, H., 2011a. The general circulation of the Gulf of Aqaba (Gulf of Eilat)
498 revisited: The interplay between the exchange flow through the Straits of Tiran and
499 surface fluxes. *J. Geophys. Res.* 116, 1–15. <https://doi.org/10.1029/2010JC006860>
- 500 Biton, E., Gildor, H., 2011b. The general circulation of the Gulf of Aqaba (Gulf of Eilat)
501 revisited: The interplay between the exchange flow through the Straits of Tiran and
502 surface fluxes. *J. Geophys. Res. Ocean.* 116, 1–15.
503 <https://doi.org/10.1029/2010JC006860>
- 504 Carlson, C.A., Hansell, D.A., Nelson, N.B., Siegel, D.A., Smethie, W.M., Khatiwala, S.,



- 505 Meyers, M.M., Halewood, E., 2010. Dissolved organic carbon export and subsequent
506 remineralization in the mesopelagic and bathypelagic realms of the North Atlantic basin.
507 Deep Sea Res. Part II Top. Stud. Oceanogr. 57, 1433–1445.
508 <https://doi.org/https://doi.org/10.1016/j.dsr2.2010.02.013>
- 509 Chen, Z., Sun, J., Gu, T., Zhang, G., Wei, Y., 2021. Nutrient ratios driven by vertical
510 stratification regulate phytoplankton community structure in the oligotrophic western
511 Pacific Ocean. Ocean Sci. 17, 1775–1789. <https://doi.org/10.5194/os-17-1775-2021>
- 512 Cheung, H.L.S., Simister, R.L., Not, C., Crowe, S.A., 2024. Microbial community respiration
513 kinetics and their dynamics in coastal seawater. Sci. Total Environ. 954, 176119.
514 <https://doi.org/https://doi.org/10.1016/j.scitotenv.2024.176119>
- 515 Dave, A.C., Lozier, M.S., 2010. Local stratification control of marine productivity in the
516 subtropical North Pacific. J. Geophys. Res. Ocean. 115.
517 <https://doi.org/https://doi.org/10.1029/2010JC006507>
- 518 de Boyer Montégut, C., Madec, G., Fischer, A.S., Lazar, A., Iudicone, D., 2004. Mixed layer
519 depth over the global ocean: An examination of profile data and a profile-based
520 climatology. J. Geophys. Res. Ocean. 109, C12003.
521 <https://doi.org/https://doi.org/10.1029/2004JC002378>
- 522 del Giorgio, P. a., Cole, J.J., 1998. Bacterial growth efficiency in natural aquatic systems.
523 Annu. Rev. Ecol. Syst. 29, 503–541. <https://doi.org/10.1146/annurev.ecolsys.29.1.503>
- 524 del Giorgio, P., Cole, J.J., Cimbleris, A., 1997. Respiration rates in bacteria exceed
525 phytoplankton production in unproductive aquatic systems. Nature 385, 148–151.
- 526 Devresse, Q., Becker, K.W., Bendinger, A., Hahn, J., Engel, A., 2022. Eddy-enhanced
527 primary production sustains heterotrophic microbial activities in the Eastern Tropical
528 North Atlantic. Biogeosciences 19, 5199–5219. [https://doi.org/10.5194/bg-19-5199-](https://doi.org/10.5194/bg-19-5199-2022)
529 2022
- 530 Dore, J.E., Letelier, R.M., Church, M.J., Lukas, R., Karl, D.M., 2008. Summer phytoplankton
531 blooms in the oligotrophic North Pacific Subtropical Gyre: Historical perspective and
532 recent observations. Prog. Oceanogr. 76, 2–38.
533 <https://doi.org/https://doi.org/10.1016/j.pocean.2007.10.002>
- 534 Duarte, C.M., Duarte, C.M., Regaudie-de-gioux, A., Agust, S., 2013. The oligotrophic ocean
535 is heterotrophic. Ann. Rev. Mar. Sci. 5, 551–569. [https://doi.org/10.1146/annurev-](https://doi.org/10.1146/annurev-marine-121211-172337)
536 marine-121211-172337
- 537 Engel, A., Bange, H.W., Cunliffe, M., Burrows, S.M., Friedrichs, G., Galgani, L., Herrmann,
538 H., Hertkorn, N., Johnson, M., Liss, P.S., Quinn, P.K., Schartau, M., Soloviev, A.,



- 539 Stolle, C., Upstill-Goddard, R.C., van Pinxteren, M., Zäncker, B., 2017. The Ocean's
540 Vital Skin: Toward an Integrated Understanding of the Sea Surface Microlayer. *Front.*
541 *Mar. Sci.* 4. <https://doi.org/10.3389/fmars.2017.00165>
- 542 Engel, A., Piontek, J., Grossart, H.P., Riebesell, U., Schulz, K.G., Sperling, M., 2014. Impact
543 of CO₂ enrichment on organic matter dynamics during nutrient induced coastal
544 phytoplankton blooms. *J. Plankton Res.* 36, 641–657.
545 <https://doi.org/10.1093/plankt/fbt125>
- 546 Engel, A., Thoms, S., Riebesell, U., Rochelle-Newall, E., Zondervan, I., 2004.
547 Polysaccharide aggregation as a potential sink of marine dissolved organic carbon.
548 *Nature* 428, 929–932. <https://doi.org/10.1038/nature02453>
- 549 Hansell, D., Carlson, C.A., Repeta, D.J., Schlitzer, R., 2009. Dissolved Organic Matter in the
550 Ocean. *Oceanography* 22, 202–11. <https://doi.org/10.5670/oceanog.2009.109>
- 551 Hansell, D.A., 2013. Recalcitrant Dissolved Organic Carbon Fractions. *Ann. Rev. Mar. Sci.*
552 5, 421–445. <https://doi.org/10.1146/annurev-marine-120710-100757>
- 553 Hansell, D.A., Carlson, C.A., 2002. Biogeochemistry of marine dissolved organic matter.
554 Academic Press, New York. <https://doi.org/10.1016/B978-0-12-323841-2.X5000-3>
- 555 Hazan, O., Silverman, J., Sisma-Ventura, G., Ozer, T., Gertman, I., Shoham-Frider, E., Kress,
556 N., Rahav, E., 2018. Mesopelagic prokaryotes alter surface phytoplankton production
557 during simulated deep mixing experiments in Eastern Mediterranean Sea waters. *Front.*
558 *Mar. Sci.* 5, 1. <https://doi.org/10.3389/fmars.2018.00001>
- 559 Holms, R., Aminot, A., K erouel, R., Hooker, B., Peterson, B., 1999. A simple and precise
560 method for measuring ammonium in marine and freshwater ecosystems. *Can. Data Rep.*
561 *Fish. Aquat. Sci.* 56, 1801–1808. <https://doi.org/10.1139/cjfas-56-10-1801>
- 562 Iluz, D., Dishon, G., Capuzzo, E., Meeder, E., Astoreca, R., Montecino, V., Znachor, P.,
563 Ediger, D., Marra, J., 2009. Short-term variability in primary productivity during a
564 wind-driven diatom bloom in the Gulf of Eilat (Aqaba). *Aquat. Microb. Ecol.* 56, 205–
565 215. <https://doi.org/10.3354/ame01321>
- 566 Izett, R.W., Fennel, K., Stoer, A.C., Nicholson, D.P., 2024. Reviews and syntheses:
567 expanding the global coverage of gross primary production and net community
568 production measurements using Biogeochemical-Argo floats. *Biogeosciences* 21, 13–47.
569 <https://doi.org/10.5194/bg-21-13-2024>
- 570 Kang, J., Luo, Z., Mohamed, H.F., Lin, Y., Huang, S., Wang, Y., Lan, W., 2022.
571 Environmental Regulation of Photosynthetically Produced Dissolved Organic Carbon by
572 Phytoplankton Along a Subtropical Estuarine Bay. *Front. Mar. Sci.* 9, 13401.



- 573 <https://doi.org/10.3389/fmars.2022.813401>
- 574 Karl, D.M., Letelier, R.M., Bidigare, R.R., Björkman, K.M., Church, M.J., Dore, J.E., White,
575 A.E., 2021. Seasonal-to-decadal scale variability in primary production and particulate
576 matter export at Station ALOHA. *Prog. Oceanogr.* 195, 102563.
577 <https://doi.org/https://doi.org/10.1016/j.pocean.2021.102563>
- 578 Kress, N., Herut, B., 2001. Spatial and seasonal evolution of dissolved oxygen and nutrients
579 in the Southern Levantine Basin (Eastern Mediterranean Sea): chemical
580 characterization of the water masses and inferences on the N : P ratios. *Deep. Res. I* 48,
581 2347–2372.
- 582 LaBrie, R., Péquin, B., Fortin St-Gelais, N., Yashayaev, I., Cherrier, J., Gélinas, Y.,
583 Guillemette, F., Podgorski, D.C., Spencer, R.G.M., Tremblay, L., Maranger, R., 2022.
584 Deep ocean microbial communities produce more stable dissolved organic matter
585 through the succession of rare prokaryotes. *Sci. Adv.* 8, eabn0035.
586 <https://doi.org/10.1126/sciadv.abn0035>
- 587 Laiolo, L., Barausse, A., Dubinsky, Z., Palmeri, L., Goffredo, S., Kamenir, Y., Al-Najjar, T.,
588 Iluz, D., 2014. Phytoplankton dynamics in the Gulf of Aqaba (Eilat, Red Sea): A
589 simulation study of mariculture effects. *Mar. Pollut. Bull.* 86, 481–493.
590 <https://doi.org/https://doi.org/10.1016/j.marpolbul.2014.06.026>
- 591 Landou, E., Lazar, B., LaRoche, J., Fennel, K., Berman-Frank, I., 2023. Contribution of
592 photic and aphotic N₂ fixation to production in an oligotrophic sea. *Limnol. Oceanogr.*
593 68, 692–708. <https://doi.org/10.1002/lno.12303>
- 594 Lindell, D., Post, A.F., 1995. Ultraphytoplankton succession is triggered by deep winter
595 mixing in the Gulf of Aqaba (Eilat), Red Sea. *Limnol. Oceanogr.* 40, 1130–1141.
596 <https://doi.org/10.4319/lo.1995.40.6.1130>
- 597 Lozier, M.S., Dave, A.C., Palter, J.B., Gerber, L.M., Barber, R.T., 2011. On the relationship
598 between stratification and primary productivity in the North Atlantic. *Geophys. Res.*
599 *Lett.* 38. <https://doi.org/https://doi.org/10.1029/2011GL049414>
- 600 Marañón, E., Behrenfeld, M.J., González, N., Mouriño, B., Zubkov, M. V., 2003. High
601 variability of primary production in oligotrophic waters of the Atlantic Ocean:
602 Uncoupling from phytoplankton biomass and size structure. *Mar. Ecol. Prog. Ser.* 257,
603 1–11. <https://doi.org/10.3354/meps257001>
- 604 Marañón, E., Fernández, A., Mouriño-Carballido, B., Martínez-García, S., Teira, E.,
605 Cermeño, P., Chouciño, P., Huete-Ortega, M., Fernández, E., Calvo-Díaz, A., Anxelu G.
606 Morán, X., Bode, A., Moreno-Ostos, E., Varela, M.M., Patey, M.D., Achterberg, E.P.,



- 607 2010. Degree of oligotrophy controls the response of microbial plankton to Saharan
608 dust. *Limnol. Oceanogr.* 55, 2339–2352. <https://doi.org/10.4319/lo.2010.55.6.2339>
- 609 Meeder, E., MacKey, K.R.M., Paytan, A., Shaked, Y., Iluz, D., Stambler, N., Rivlin, T., Post,
610 A.F., Lazar, B., 2012. Nitrite dynamics in the open ocean-clues from seasonal and
611 diurnal variations. *Mar. Ecol. Prog. Ser.* 453, 11–26. <https://doi.org/10.3354/meps09525>
- 612 Mentges, A., Feenders, C., Deutsch, C., Blasius, B., Dittmar, T., 2019. Long-term stability of
613 marine dissolved organic carbon emerges from a neutral network of compounds and
614 microbes. *Sci. Rep.* 9, 17780. <https://doi.org/10.1038/s41598-019-54290-z>
- 615 Morana, C., Sarmiento, H., Descy, J.-P., Gasol, J.M., Borges, A. V, Bouillon, S.,
616 Darchambeau, F., 2014. Production of dissolved organic matter by phytoplankton and its
617 uptake by heterotrophic prokaryotes in large tropical lakes. *Limnol. Oceanogr.* 59,
618 1364–1375. <https://doi.org/https://doi.org/10.4319/lo.2014.59.4.1364>
- 619 Mueller, B., den Haan, J., Visser, P.M., Vermeij, M.J.A., van Duyl, F.C., 2016. Effect of light
620 and nutrient availability on the release of dissolved organic carbon (DOC) by Caribbean
621 turf algae. *Sci. Rep.* 6, 23248. <https://doi.org/10.1038/srep23248>
- 622 Ofaim, S., Sulheim, S., Almaas, E., Sher, D., Segrè, D., 2021. Dynamic allocation of carbon
623 storage and nutrient-dependent exudation in a revised genome-scale model of
624 *Prochlorococcus*. *Front. Genet.* 12, 586293. <https://doi.org/10.3389/fgene.2021.586293>
- 625 Paytan, A., Mackey, K.R.M., Chen, Y., Lima, I.D., Doney, S.C., Mahowald, N., Labiosa, R.,
626 Post, A.F.A.F., 2009. Toxicity of atmospheric aerosols on marine phytoplankton. *Proc.*
627 *Natl. Acad. Sci. U. S. A.* 106, 4601–5. <https://doi.org/10.1073/pnas.0811486106>
- 628 Pennington, J.T., Mahoney, K.L., Kuwahara, V.S., Kolber, D.D., Calienes, R., Chavez, F.P.,
629 2006. Primary production in the eastern tropical Pacific: A review. *Prog. Oceanogr.* 69,
630 285–317. <https://doi.org/https://doi.org/10.1016/j.pocean.2006.03.012>
- 631 Polovina, J.J., Howell, E. a., Abecassis, M., 2008. Ocean’s least productive waters are
632 expanding. *Geophys. Res. Lett.* 35, 2–6. <https://doi.org/10.1029/2007GL031745>
- 633 Rahav, E., Giannetto, M., Bar-Zeev, E., 2016. Contribution of mono and polysaccharides to
634 heterotrophic N₂ fixation at the eastern Mediterranean coastline. *Scientific Reports* 6,
635 27858. <https://doi.org/10.1038/srep27858>
- 636 Rahav, E, Herut, B., Mulholland, M., Belkin, N., Elifantz, H., Berman-Frank, I., 2015.
637 Heterotrophic and autotrophic contribution to dinitrogen fixation in the Gulf of Aqaba.
638 *Mar. Ecol. Prog. Ser.* 522, 67–77. <https://doi.org/10.3354/meps11143>
- 639 Rahav, Eyal, Herut, B., Mulholland, M.R., Belkin, N., Elifantz, H., Berman-Frank, I., 2015.
640 Heterotrophic and autotrophic contribution to dinitrogen fixation in the Gulf of Aqaba.



- 641 Mar. Ecol. Prog. Ser. 522, 67–77. <https://doi.org/10.3354/meps11143>
- 642 Rahav, E., Paytan, A., Mescioglu, E., Galletti, Y., Rosenfeld, S., Raveh, O., Santinelli, C.,
643 Ho, T.Y., Herut, B., 2018. Airborne Microbes Contribute to N₂ Fixation in Surface
644 Water of the Northern Red Sea. *Geophys. Res. Lett.* 45, 6186–6194.
645 <https://doi.org/10.1029/2018GL077132>
- 646 Redfield, A.C., 1934. On the proportions of organic derivatives in sea water and their relation
647 to the composition of plankton. University Press of Liverpool Liverpool.
- 648 Reich, T., Belkin, N., Sisma-Ventura, G., Berman-Frank, I., Rahav, E., 2024. Significant dark
649 inorganic carbon fixation in the euphotic zone of an oligotrophic sea. *Limnol. Oceanogr.*
650 9999, 1–14. <https://doi.org/10.1002/lno.12560>
- 651 Reich, T., Belkin, N., Sisma-ventura, G., Hauzer, H., Berman-frank, I., Rahav, E., 2026. Does
652 oligotrophy favor chemoautotrophy over photoautotrophy? *Prog. Oceanogr.* 241,
653 103633. <https://doi.org/10.1016/j.pocean.2025.103633>
- 654 Reich, T., Ben-ezra, T., Belkin, N., Tsemel, A., Aharonovich, D., Roth-rosenberg, D., Givati,
655 S., Bialik, M., Herut, B., Berman-frank, I., Frada, M., Krom, M.D., Lehahn, Y., Rahav,
656 E., Sher, D., 2022. A year in the life of the Eastern Mediterranean : Monthly dynamics
657 of phytoplankton and bacterioplankton in an ultra-oligotrophic sea. *Deep. Res. Part I*
658 182, 103720. <https://doi.org/10.1016/j.dsr.2022.103720>
- 659 Roshan, S., DeVries, T., 2017. Efficient dissolved organic carbon production and export in
660 the oligotrophic ocean. *Nat. Commun.* 8, 2036. [https://doi.org/10.1038/s41467-017-](https://doi.org/10.1038/s41467-017-02227-3)
661 [02227-3](https://doi.org/10.1038/s41467-017-02227-3)
- 662 Santinelli, C., 2015. DOC in the Mediterranean Sea, in: Hansell, D.A., Carlson, C.A. (Eds.),
663 Biogeochemistry of Marine Dissolved Organic Matter. Academic Press, London, pp.
664 579–608. <https://doi.org/10.1016/B978-0-12-405940-5.00013-3>
- 665 Signorini, S.R., Franz, B.A., McClain, C.R., 2015. Chlorophyll variability in the oligotrophic
666 gyres: Mechanisms, seasonality and trends. *Front. Mar. Sci.* 2, 1–11.
667 <https://doi.org/10.3389/fmars.2015.00001>
- 668 Simon, M., Alldredge, A.L., Azam, F., 1990. Bacterial carbon dynamics on marine snow.
669 *Mar. Ecol. Prog. Ser.* 65, 205–211.
- 670 Simon, M., Azam, F., 1989. Protein-content and protein-synthesis rates of planktonic marine-
671 bacteria. *Mar. Ecol. Prog. Ser.* 51, 201–213.
- 672 Smith, D.C., Azam, F., 1992. A simple, economical method for measuring bacterial protein
673 synthesis rates in seawater using tritiated-leucine. *Mar. Microb. Food Webs* 6, 107–114.
- 674 Stanley, R.H.R., Kirkpatrick, J.B., Cassar, N., Barnett, B.A., Bender, M.L., 2010. Net



- 675 community production and gross primary production rates in the western equatorial
676 Pacific. *Global Biogeochem. Cycles* 24, GB4001.
677 <https://doi.org/https://doi.org/10.1029/2009GB003651>
- 678 Tanioka, T., Garcia, C.A., Larkin, A.A., Garcia, N.S., Fagan, A.J., Martiny, A.C., 2022.
679 Global patterns and predictors of C:N:P in marine ecosystems. *Commun. Earth Environ.*
680 3, 271. <https://doi.org/10.1038/s43247-022-00603-6>
- 681 Thornton, D.C.O., 2014. Dissolved organic matter (DOM) release by phytoplankton in the
682 contemporary and future ocean. *Eur. J. Phycol.* 49, 20–46.
683 <https://doi.org/10.1080/09670262.2013.875596>
- 684 Torfstein, A., Kienast, S.S., Yarden, B., Rivlin, A., Isaacs, S., Shaked, Y., 2020. Bulk and
685 Export Production Fluxes in the Gulf of Aqaba, Northern Red Sea. *ACS Earth Sp.*
686 *Chem.* 4, 1461–1479. <https://doi.org/10.1021/acsearthspacechem.0c00079>
- 687 Welschmeyer, N.A., 1994. Fluorometric analysis of chlorophyll a in the presence of
688 chlorophyll b and pheopigments. *Limnol. Oceanogr.* 39, 1985–1992.
- 689 Zhang, Y., Huang, Y., Xu, F., Cai, S., Liu, Y., Xu, C., Lin, L., Chen, J., Laws, E.A., Liu, X.,
690 Huang, B., 2025. Decoupling of bacterial production and respiration in the surface water
691 of the North Pacific Subtropical Gyre. *Mar. life Sci. Technol.* 7, 397–412.
692 <https://doi.org/10.1007/s42995-025-00279-9>
- 693 Zohary, T., Herut, B., Krom, M.D., Fauzi C. Mantoura, R., Pitta, P., Psarra, S.,
694 Rassoulzadegan, F., Stambler, N., Tanaka, T., Frede Thingstad, T., Malcolm S.
695 Woodward, E., 2005. P-limited bacteria but N and P co-limited phytoplankton in the
696 Eastern Mediterranean - A microcosm experiment. *Deep. Res. Part II Top. Stud.*
697 *Oceanogr.* 52, 3011–3023. <https://doi.org/10.1016/j.dsr2.2005.08.011>